BBA - Proteins and Proteomics 1866 (2018) 661–667

Contents lists available at ScienceDirect

BBA - Proteins and Proteomics

journal homepage: www.elsevier.com/locate/bbapap

Rhodamine binds to silk fibroin and inhibits its self-aggregation

Laura Ragona[a,*], Oktay Gasymov[b], Aytaj J. Guliyeva[b], Rasim B. Aslanov[b], Serena Zanzoni[c], Chiara Botta[a], Henriette Molinari[a,*]

[a] Istituto per lo Studio delle Macromolecole (ISMAC), CNR, via Corti 12, 20133 Milano, Italy
[b] Institute of Biophysics of ANAS, 117 Khalilov, AZ-1141 Baku, Azerbaijan
[c] Department of Biotechnology, University of Verona, Strada Le Grazie 15, 37134 Verona, Italy

ARTICLE INFO

Keywords:
Silk fibroin
Self-aggregation
NMR spectroscopy
Gelation/fibril formation
Aggregation inhibition
Ligand binding

ABSTRACT

Amyloid structures are universal structures, widely diffuse in nature. Silk, capable of forming some of the strongest tensile materials on earth represents an important example of formation of functional amyloid fibrils, a process reminiscent of the oligomerization of peptides involved in neurodegenerative diseases. The stability of silk fibroin solutions in different conditions and its transition from α-helix/random coil to β-sheet structures, at the basis of gelation processes and fibril formation, have been here investigated and monitored employing different biophysical approaches. Silk fibroin aggregation state as a function of concentration, pH and aging has been characterized employing NMR ordered diffusion spectroscopy. The change of silk fibroin diffusion coefficient over time, which reflects the progress of oligomerization, has been monitored for silk fibroin alone and in the presence of a polycondensed aromatic dye, namely rhodamine 6G. NMR, UV and DLS measurements indicated that rhodamine specifically binds to silk fibroin with a micromolar K_D. The reported data reveal, for the first time, that RHD is capable of inhibiting fibroin self-association, thus controlling β-conformational transition at the basis of fibril formation. The described approach could be extended to further protein systems, allowing better control of the oligomerisation process.

1. Introduction

Silk fibroin (SF) from *Bombyx mori*, a protein-based polymer with reported excellent mechanical properties and biocompatibility [1–6], is widely investigated either for its promising applications in different fields, from optoelectronics to neurodegenerative medicine and as a model of protein assembly into functional fibrils [7,8].

It has now become increasingly clear that many proteins possess an intrinsic propensity, in appropriate conditions, towards amyloid formation and amyloids are now recognized as an integral structural and functional entity in all forms of life [9]. Silk, capable of forming some of the strongest tensile materials on earth [10], thus represents an important example of formation of functional amyloid fibrils. In a growing effort to understand functional versus aberrant fibrillation, an important field of research is related to the study of the different molecular mechanisms and biological functions of amyloid-forming proteins [9,11]. These studies are aimed to understanding the mechanisms in place to ensure that potentially adverse intermediates are not formed. Silk fibroin assembly, here addressed, appears to display the most intricate autoregulatory properties, still in high demand for clarification.

SF can be extracted from *Bombyx mori* cocoons by removing sericin, the soluble glycoprotein component, from the core of fibroin fibers. Fibroin consists of a heavy (H) (390 KDa) and a light (L) (26 KDa) chain, which are connected by a disulphide bond. The H chain is essentially composed by four modular motifs, namely a highly repetitive GAGAGS sequence (the crystalline region), two less repetitive sequences containing hydrophobic units, such as GAGAGY, GAGAGV and GAGAGVGY (the semi-crystalline regions) and an amorphous region containing charged bulky or aromatic side-chains [2]. The presence of predominantly hydrophobic blocks leads to extensive hydrogen and hydrophobic interactions throughout the protein chains resulting in homogeneous secondary structure, imparting crystallinity to the protein. Less organized domains of 34–40 amino acids are interspersed with the highly crystalline regions, giving rise to fibers with a remarkable strength and elasticity [12]. X-ray solid state characterization of SF has provided only limited structural information because SF exists as a fiber form, not as a single crystal, and the packing structure is heterogeneous and not easy to study [13]. Solid state NMR studies have reported two kinds of crystalline modifications, Silk I, a metastable and water soluble conformation and Silk II, the water-insoluble structure stabilized after silkworm spinning and found in cocoon fibers [2,3]. Silk I comprises random coil/α-helix soluble species which progressively

* Corresponding authors.
E-mail addresses: laura.ragona@ismac.cnr.it (L. Ragona), henriette.molinari@univr.it (H. Molinari).

https://doi.org/10.1016/j.bbapap.2018.03.009
Received 16 January 2018; Received in revised form 16 March 2018; Accepted 22 March 2018
Available online 02 April 2018

convert to beta-sheet structures, a process at the basis of SF gelation and fibril formation. Silk fibroin, processed from aqueous solutions [14], adopts the same structure found in the silkworm gland [14,15], i.e. Silk I. The predominance in SF of hydrophobic amino acid groups makes gelation (namely the conversion to beta sheet structures) possible without addition of any gelling agent, thus strongly affecting the stability of the "monomeric" species in solution [16,17]. Increase of SF concentration (from 1 to > 8 *w/v*%) affects aggregation/gelation processes leading to a decrease of the fast segmental motions exhibited both in aqueous solution and in the silkworm gland [18–20].

SF conformational transition to beta-sheet structures have been recognized to parallel beta-sheet driven oligomerization processes, which play a relevant role in fibril formation of proteins involved in neurodegenerative diseases [7,11,21,22].

The “life-time”/stability of the monomeric random coil conformation of SF, as a function of concentration, pH and aging, has been here investigated employing NMR ordered diffusion spectroscopy. The role of small ligands as self-aggregation inhibitors, able to interfere with SF β-conformational transition, has been further explored. A fluorescent polycondensed aromatic molecule, Rhodamine 6G (RHD), was previously shown to be a versatile doping molecule to be incorporated into silk fibroin, by means of silk worms feeding, to obtain bio-derived materials [23]. We were therefore interested in the investigation, in solution, of SF interactions with RHD. Collectively our results reveal that RHD displays a specific binding to silk fibroin, successfully inhibiting protein time-dependent self-aggregation. These findings can be extended to investigations on other proteins, with the aim of preventing and/or decreasing their aggregation.

2. Results and discussion

2.1. Oligomerisation properties of silk fibroin

Preparation of silk fibroin solution was performed as described [14]. ^{1}H 1D NMR and 2D TOCSY and NOESY experiments, initially performed at 25 °C, for samples obtained following the above-mentioned protocol, were consistent with data reported in the literature [2] (Fig. S1, S2). However, after 48 h at 25 °C, the 1.5 *w/v* % sample turned towards a gel. In order to preserve SF solutions for a longer time, all NMR experiments were conducted at 12 °C. Different SF concentrations, in the range 2.5–22 μM, were tested and the obtained ^{1}H 1D spectra are reported in Fig. 1.

The only observed effect on SF resonances was the expected intensity reduction, upon dilution. No change in SF ^{1}H chemical shift

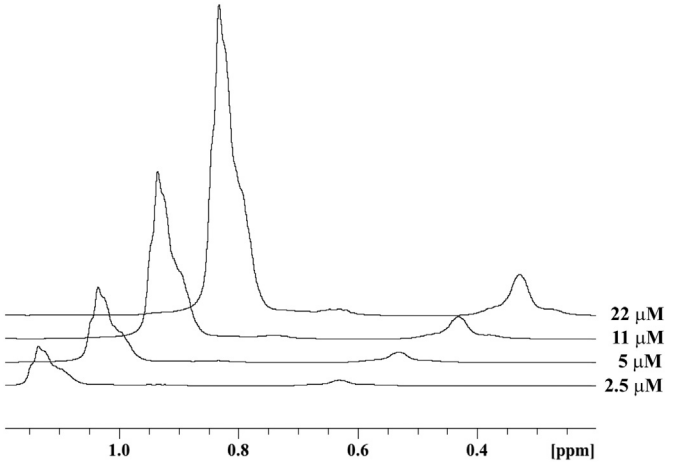

Fig. 1. ^{1}H 1D spectra of SF. Stacked plot of the methyl region of ^{1}H 1D spectra of SF samples at increasing concentrations. A horizontal shift of 0.1 ppm was employed to better visualize the change in intensity of each peak.

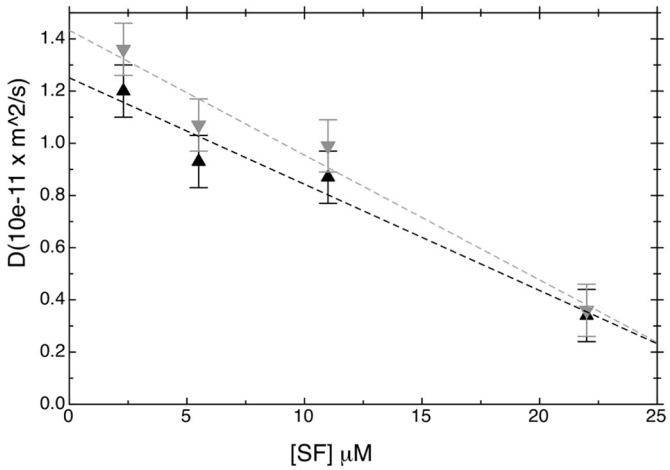

Fig. 2. Diffusion as a function of SF concentration. Diffusion values of the main aliphatic (black) and aromatic (grey) components of SF samples at different concentrations, as deduced from 2D-DOSY experiments at 12 °C and pH 6. Error bars refer to the standard deviation of measurements performed in triplicate.

and/or linewidth, possibly reflecting different aggregation states as a function of concentration, was observed in the analyzed concentration range (0.2–1.5 *w/v*%). Previous data indicated as well that no ^{13}C chemical shift change was observed on going from dilute aqueous solution (2 *w/v*%) to “liquid silk” concentrations (30 *w/v*%) [19]. Thus, neither chemical shift perturbation nor signal linewidth represent useful probes to monitor SF oligomerization state. Diffusion experiments were therefore employed to monitor SF self-aggregation.

Diffusion ordered NMR spectroscopy (DOSY) provides a powerful tool for the analysis of aggregation, mixtures, and protein-ligand complexes, since each resonance gives rise to one or more signals in the diffusion dimension, depending on the diffusion coefficient of the contributing components. The obtained diffusion values thus reveal the distribution of molecular sizes at each frequency in the NMR spectrum. Pseudo 2D diffusion ordered NMR spectra (2D-DOSY), recorded on SF samples at different concentration, revealed a progressive disaggregation upon dilution, as reflected in the measured faster translational diffusion coefficients (Fig. S3). As an example, the reported range of diffusion for aliphatic and aromatic resonances is reported for all tested concentration in Fig. 2.

It is clear that the highest effect, in terms of decreased oligomerization, is observed on going from 22 to 11 μM, with D values which increases from 0.35 ± 0.05 to 0.87 ± 0.04 × 10^{-11} m^2/s, (for the aliphatic resonance) indicating a three-fold increase of the diffusion upon dilution. Further dilutions to 5 and 2.5 μM do not change substantially the oligomerization status, and represent a disadvantage with respect to the lower S/N obtained for NMR analysis. A concentration of ca. 10 μM was therefore considered the best compromise for the different experiments to be performed by NMR.

The reported protocol for obtaining regenerated SF [14] included sample dialysis against water, thus leading to a solution with pH ca. 6, which favors SF aggregation. Indeed it has been reported that the N-terminal domain is highly sensitive to changes in pH, facilitating fiber formation at low pH [24,25]. The effect of pH on SF aggregation could be deduced from 2D-DOSY experiments (Fig. 3).

The hydrodynamic radius of a protein/assembly could in principle be estimated from the diffusion coefficient by using the Stokes–Einstein equation, with the assumption that the protein is spherical [26,27]. Although we are aware that this assumption may not be valid for disordered peptides [28], as is the case for silk fibroin, the rough estimate of the molecular weight/hydrodynamic radii, and therefore of the oligomerization state, was inferred from 2D-DOSY data. At pH 6 heterogeneous multimeric species, formed by 15 to 40 SF monomers, are

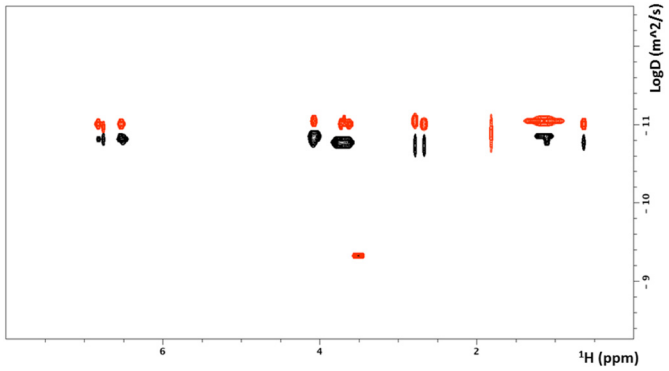

Fig. 3. Effect of pH on SF oligomerization state. Superposition of the 2D-DOSY spectrum of a 11 μM SF sample at 12 °C and pH 6.0 (red) and of the same sample where pH was adjusted to 8.6 by addition of 2 μL of 100 mM NaOH (black).

present in solution as evaluated on the basis of 2D-DOSY spectra. The increase of the solution pH of two units (8.5) stabilizes smaller oligomers including dimers and trimers (Fig. 3). We can therefore suggest that, in order to stabilize monomeric species and investigate the net effect of added ligands on oligomerisation, it is important to work at a controlled pH. Thus an optimized protocol to obtain sample solutions with a low content of aggregated species, requires: 1) SF starting solutions with concentrations lower than 1.5 *w/v* %; 2) dialysis against phosphate buffer at physiological pH around 7.5 and low ionic strength; 3) short dialysis time (up to 12 h).

2.2. UV and NMR data show that RHD binds to SF

SF/RHD interaction properties, in terms of specificity and stoichiometry of binding, have been here investigated employing titration experiments followed by optical and NMR measurements.

UV titration experiments were first performed keeping the concentration of RHD constant (2 μM) and varying SF concentration from 0 to 40 μM, in order to identify the spectral characteristics of RHD in the bound form (Fig. 4). Absorption spectra of RHD exhibited a red shift with a decreased molar extinction, upon binding to SF. A fairly good isosbestic point in the titration experiment was observed at 533.7 nm (Fig. 4A), suggesting the presence of an equilibrium between RHD free and bound forms. The titration experiments were performed employing up to 20-fold excess of SF over the dye concentration to ensure that all RHD molecules were bound at the end of the titration. Indeed, red shift of absorption maximum reached a plateau at 534 nm, corresponding to bound RHD (Fig. 4B).

A complementary titration experiment was performed incubating increasing concentrations of RHD with a 5 or 11 μM SF sample. Progressive addition of RHD resulted in a blue shift of the spectra due to the contribution of the free ligand. The difference in the absorption maxima of RHD in bound and free forms was used to estimate RHD dissociation constant employing Eq. (1) [29].

$$RHD_{bound}/(RHD_{free} \times [SF]) = (1/K_D) \times n - (1/K_D) \times (RHD_{bound}/[SF])$$
$$RHD_{bound} = (\lambda_{obs}-\lambda_{free}/\lambda_{max}-\lambda_{free}) \times RHD_{tot} \quad (1)$$

where RHD_{bound}, RHD_{free} and RHD_{tot} are bound, free and total RHD concentrations. [SF] is the concentration of silk fibroin and n is stoichiometry. λ_{obs} represents the wave-length of the absorption maxima measured along the titration. λ_{free} and λ_{max} refer to free and bound RHD absorption maxima, respectively. Free ligand concentration is defined as $RHD_{free} = RHD_{tot}-RHD_{bound}$. K_D is the dissociation constant.

Specifically, K_D of 31.2 μM and 47.1 μM and stoichiometry of 5.0 and 5.7 were deduced from the analysis of the interaction data on SF samples at 5 and 11 μM, respectively (Fig. 5). Altogether these data indicate the presence of a specific binding of the dye to SF. It should be stressed that under the experimental conditions employed for the binding studies the monomeric species mostly accounts for ≥90% of the total RHD and the influence of RHD dimer formation is negligible [30,31].

Fluorescence experiments were also performed at 1 μM RHD, in the presence of increasing amounts of SF up to 32 μM. A gradual red shift of RHD fluorescence maximum, upon SF addition, indicates changes in the environment of the chromophore, confirming that RHD binds to SF (Fig. S4). The observed non-saturating red shift is consistent with the affinity properties of the SF:RHD system (Kd = 30 μM, n = 5), as obtained with absorption measurements.

NMR diffusion experiments have been used as well to monitor RHD binding to SF. The resonances of a small molecule, which does not interact with the protein, are expected at the diffusion coefficient of the free molecule, as is the case for dioxane, added to the sample as internal reference. In case of binding two situations may occur, depending on the timescale of the exchange process taking place between the protein and the ligand, during the diffusion sensitive period. For slow exchange the signal of the free ligand will be observable, at the diffusion coefficient of the free molecule, only after saturation of the receptor binding sites. At variance, if the small molecule is in fast exchange with the receptor, a single species will be expected in the 2D-DOSY spectrum, at the average D value of the exchanging species.

A series of NMR experiments were performed at low SF concentration (0.1 μM) to allow the investigation of RHD:SF ratios higher than the stoichiometry (deduced from optical measurements), maintaining the maximum ligand concentration below 10^{-5} M, to avoid sample precipitation and to ensure the presence of monomeric RHD. Indeed we

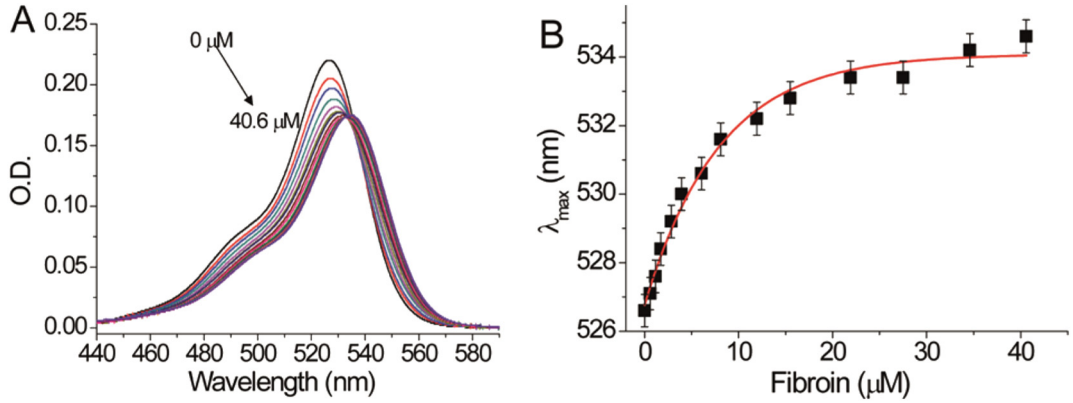

Fig. 4. RHD binding to fibroin. (A) Absorption spectra of RHD (2 μM) in the presence of increasing concentrations of SF in the range 0–40.6 μM. (B) Dependence of the wavelength of RHD absorption maximum (λ_{max}) as a function of SF concentration. Error bars in Fig. 4B refer to the standard deviation over measurements done in triplicate.

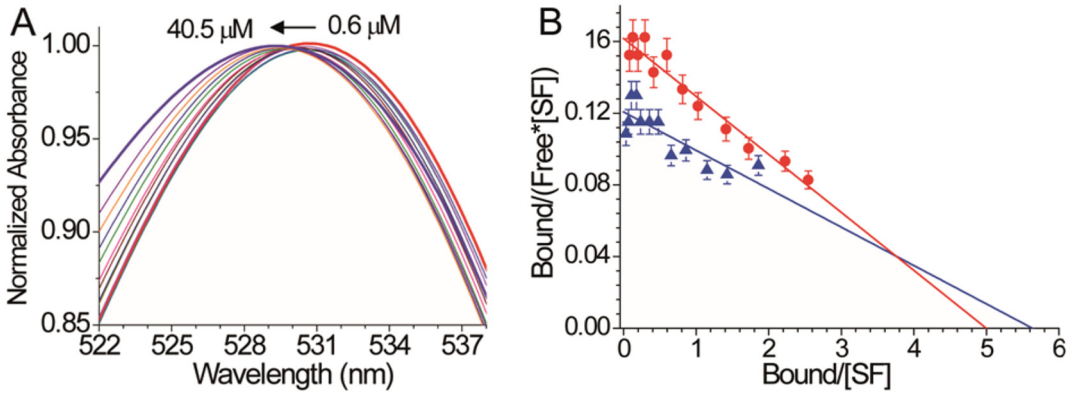

Fig. 5. Binding of RHD to SF. (A) Normalized absorption spectra of RHD at different concentrations incubated with SF (5 μM). The arrow on panel A indicates the shift of the spectra upon increasing RHD concentrations. (B) Scatchard plots for the binding of RHD to SF using 5 μM (red) and 11 μM (blue) protein samples. Data were fitted according to Eq. (1); legends "Bound" and "Free" in panel B refer to RHD_{bound} and RHD_{free}. Error bars in Fig. 4B refer to the standard deviation over measurements done in triplicate.

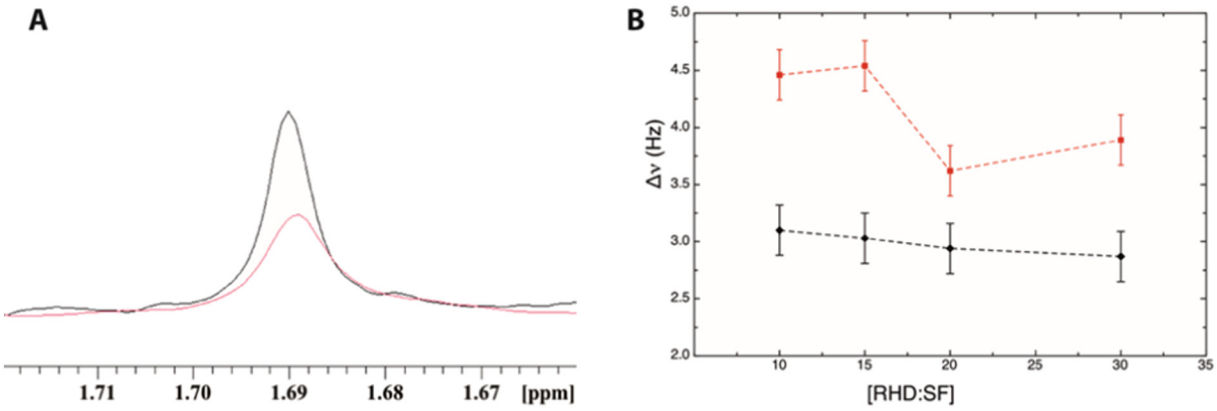

Fig. 6. RHD linewidth broadening in the presence of SF. A) Zoom on methyl ortho resonance in the ^{1}H 1D spectrum of RHD in the complex RHD:SF at 10 molar ratio (red) superimposed on the spectrum of RHD alone at the same concentration (black); B) Resonance linewidth change as a function of RHD:SF molar ratio as obtained for RHD in the presence of SF (red) and in control samples containing RHD alone (black) at the same concentrations employed for complexes. Error bars represent the digital resolution.

have previously shown, by optical absorption measurements, that RHD remains monomeric up to concentrations lower than 10^{-5} M [30]. RHD resonances were clearly observable in ^{1}H 1D spectra at RHD:SF molar ratios higher than 5. Linewidth broadening of ~2 Hz, observed for RHD signal at 1.8 ppm (free from overlap with protein resonances) in the presence of SF at RHD:SF molar ratio of 10, provides clear evidence of binding. Resonance linewidth decreased upon increasing RHD:SF molar ratios up to 30, in line with the increased concentration of unbound RHD (Fig. 6A). Control experiments, performed on RHD alone at the same concentration of each tested molar ratio, indicated no change in linewidth upon increasing RHD concentration (Fig. 6B).

2D-DOSY experiments were also performed on these samples, employing a diffusion delay period optimized for the detection of the small ligand. Resonances of unbound RHD, characterized by diffusion coefficients typical of small oligomeric species (from dimers to tetramers) were observed pointing to the presence of a protein-ligand slow exchange regime on the NMR time-scale. As an example the DOSY spectrum obtained at RHD:SF 20 is reported in Fig. 7.

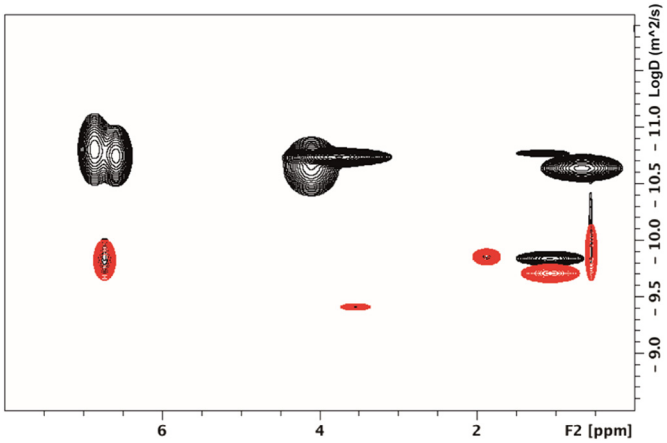

Fig. 7. Pseudo 2D-DOSY experiments performed at SF concentration 0.1 μM. Superposition of selected regions of spectra obtained at RHD:SF 20 (black) with RHD alone (red) at the same concentration of the corresponding complex. Dioxane (as internal reference) has a diffusion coefficient at 12 °C in D_2O of $3.91 \pm 0.1 \times 10^{-10}$ m^2/s (Log D is reported on F1 axis). RHD alone (red) exhibits resonances with diffusion coefficients of $1.42 \pm 0.11 \times 10^{-10}$ and $1.95 \pm 0.29 \times 10^{-10}$ m^2/s corresponding to tetramers and dimers, respectively. The DOSY spectrum at RHD:SF 20 (black) shows the resonances of unbound tetrameric RHD.

2.3. RHD controls SF oligomerization state

The comparison of 2D-DOSY spectra, optimized for protein observation and recorded in the absence and in the presence of RHD, clearly shows that the diffusion coefficient of the main observable species increases in the presence of RHD (Fig. 8).

These experiments reveal for the first time the ability of RHD to

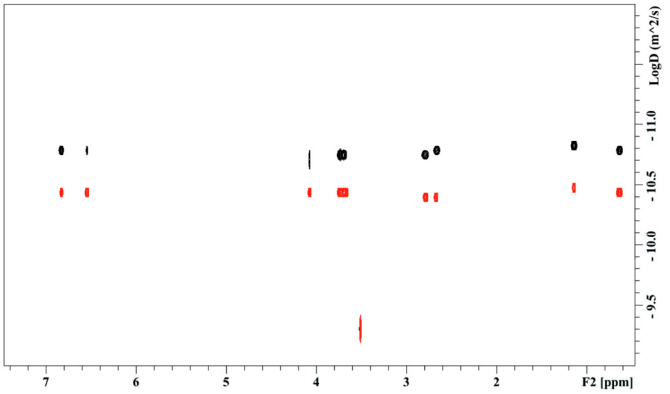

Fig. 8. RHD promotes SF disaggregation of fresh SF sample. Superposition of 2D-DOSY spectra of SF in the absence (black) and in the presence of RHD (RHD:SF 5) (red) after 3 days at 12 °C.

humper SF oligomerization occurring with time. A control 2D-DOSY experiment, repeated on RHD:SF 5 sample after 30 days, revealed the same distribution of molecular species.

A rough estimate of the effective hydrodynamic radius of protein oligomeric species was attempted using the small dioxane molecule as an internal standard and assuming a spherical model [32–34]. The principal NMR visible oligomeric species of apo SF show hydrodynamic radius ranging from 4.9 to 7.1 nm, depending on the aging of the sample. These figures were validated by DLS measurements yielding a SF average diameter of 10.9 nm (Fig. S5). A substantial increase in the diffusion value was observed in the presence of RHD, pointing to significant decrease in the hydrodynamic radius, in spite of the approximation introduced with the spherical assumption (Table 1).

This behavior proofs the ability of the hydrophobic dye to stabilize "monomeric" species, partially shielding the hydrophobic interactions, responsible for self-aggregation.

2.4. SF oligomerization over time, without and with RHD, is monitored by NMR

2D-DOSY experiments, allowing the estimate of the molecular size present in solution, require a long acquisition time (6–12 h) and are therefore not appropriate to follow a rapidly changing sample. The oligomerization behavior of SF over time could be successfully monitored recording a series of 1D-diffusion experiments, optimized for SF observation, at a fixed gradient strength. This kind of experiments is based on the accumulation, after a diffusion period, of spin phase differences, which is related to the positions of atoms during the diffusion time. Thus, faster diffusion means that the spins can travel farther and, in the presence of a magnetic field gradient, experience larger magnetic field changes. The faster diffusion thus causes larger phases spread and results in a smaller signal. Slower diffusion give rises to the opposite effect [35]. The short acquisition time of the experiment (minutes rather than hours) makes it a versatile tool to follow SF oligomerization. As an example, the behavior of SF methyl resonances occurring at 1.17 ppm is depicted in Fig. 9, in comparison with the corresponding 1D ^{1}H spectra, recorded after the same time period. The data highlight the power of 1D diffusion spectra to elucidate an underlying change, which could not be detected by simple ^{1}H-1D spectra.

1D diffusion data, followed over time, reported on an increase of SF signal intensity for all the resonances, already within the first 20 h after sample preparation. This behavior is caused by the population growth of high aggregated species, exhibiting slower diffusion. At variance, as mentioned, no change in intensity and/or signal linewidth is observed in simple ^{1}H 1D SF spectra, which monitor fast segmental local motions (also in the presence of high molecular size aggregates).

SF aggregation behavior in the absence and in the presence of RHD, monitored over time through 1D diffusion measurements, is reported in Fig. 10. After an equilibration time of ca. 180 min, a progressive increase of peak intensity with time (reflecting the presence of increasing molecular weight species) was observed for the apo SF sample. At variance, when RHD is added to a freshly prepared SF sample, self-aggregation is inhibited (Fig. 10, red circles). When RHD was added to an aged sample (kept for five days at 4 °C), the observation of inhibitory effects requires a longer time, consistent with the competition with early stages of gelation (Fig. 10, green squares).

Table 1
Range of diffusion values (D) and estimates of hydrodynamic radii (R_h) of the main NMR observable species in solution[a].

Sample	D (m^2/s)	R_h (nm)
SF	$1.65 \pm 0.30 \times 10^{-11}$	4.9–7.1
RHD:SF 5	$3.15 \pm 0.51 \times 10^{-11}$	3.0–4.2

[a] D values are given as the average of diffusion values obtained over different samples prepared with the same procedure. The error represents the standard deviation calculated over at least three data sets.

3. Conclusions

SF has gained attention as a biomaterial because of several desirable properties, which include its biocompatibility, the ease with which it can be chemically modified, its slow rate of degradation in vivo and its ability to be processed into multiple material formats from either aqueous solution or organic solvents [14]. SF is also a useful model for protein assembly into functional fibrils. The principal aim of this investigation on SF aggregation properties, under different conditions (concentration, pH, and aging), as well as in the presence of a poly-condensed aromatic inhibitor (rhodamine 6G), was to understand the molecular mechanism that proteins use to control their own assembly into oligomers.

Very simple diffusion-based NMR spectroscopic techniques were efficiently employed to monitor the protein oligomerization kinetics, the reversibility of the process and its dependence on the specificity of the interaction with a ligand.

An optimized protocol for the preparation of SF samples, characterized by reduced aggregation states, has been here proposed. The time-dependence of SF oligomerization, followed in the absence and in the presence of RHD, demonstrated that RHD binds to silk fibroin with K_D in the 30–40 micromolar range and acts as an inhibitor of SF self-aggregation. It is likely that RHD may form π-stacking interactions with aromatic tyrosine side-chains, thus stabilizing the Silk I conformation. Indeed the role of tyrosine residues in influencing the intermolecular chain arrangement in SF has been previously recognized, showing that tyrosine exerts long-range packing effects in the semi-crystalline regions of silk fibers [36]. In this line, π-interactions involving this residue can exert an important effect on the resulting structure.

The inhibition of aggregation has been shown to be at work for a freshly prepared SF sample or in the early phases of gelation, in analogy with the behavior reported for amyloid peptides, whose oligomerization kinetics strongly depends on the oligomerization state of the starting material. The presented results, demonstrating that RHD specifically interferes with a nucleation-dependent aggregation mechanism, can find applications in the study of protein aggregation processes, providing an approach aimed at preventing or decreasing aggregation.

The discussed results are also relevant for the controlled formation of silk fibroin nano-assemblies, which bears relevance for the optimization of protein-based biomaterials [23,30,37] whereby the ability to tune the features of the final biomaterial is based on the molecular knowledge of the interactions between the dye and the protein assemblies.

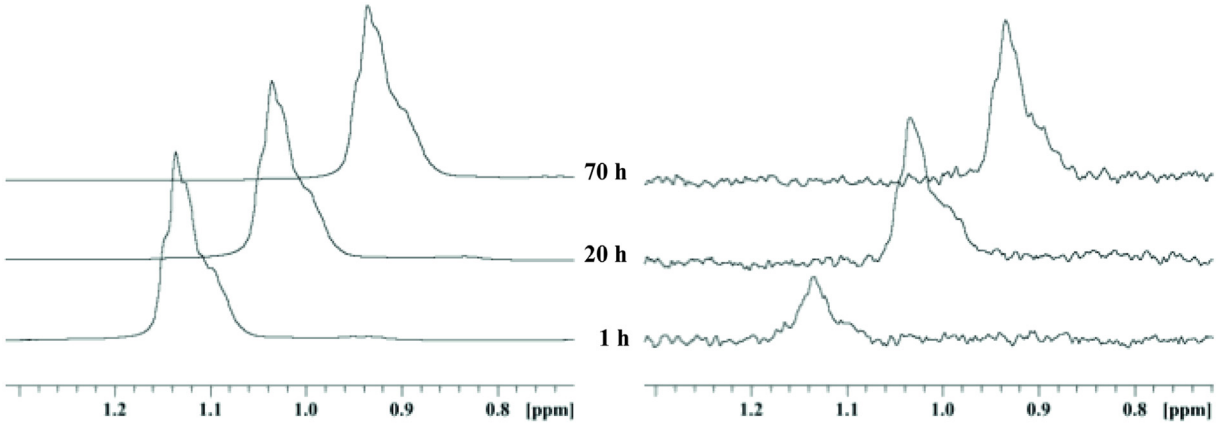

Fig. 9. ^{1}H 1D versus 1D DOSY NMR experiments. Methyl resonances intensity of a 11 μM SF sample as a function of time (hours) as measured in 1D spectra (left panel) and in 1D diffusion spectra (right panel). A horizontal shift of 0.1 ppm was employed to better visualize the change in intensity of each peak.

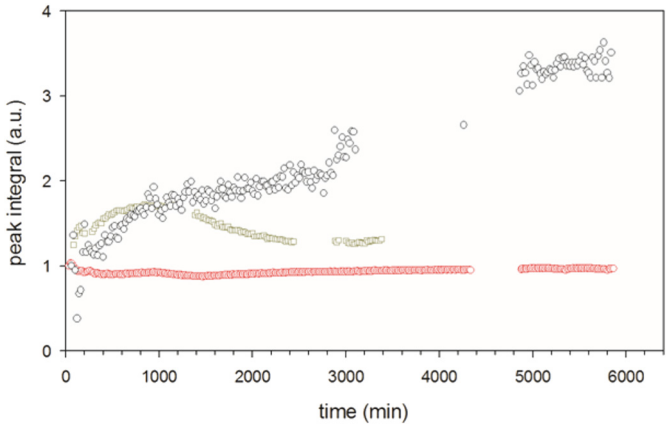

Fig. 10. Effect of RHD on SF oligomerization state. Comparison of the change of SF methyl intensity in 1D diffusion experiments, at fixed gradient strength, vs time for: i) fresh apo SF (black circle); ii) SF in the presence of RHD (RHD:SF 5), with the dye added to a freshly prepared SF sample, immediately after dialysis (red circle) or to a SF sample stored for 5 days at 4 °C (green squares). The absence of data points in some time intervals is due to the acquisition of 2D-DOSY.

4. Materials and methods

4.1. Sample preparation

Fibroin was obtained from the silk cocoons of *Bombyx mori* following a widely used standard procedure [14]. Silk cocoons were cut into small pieces and then boiled for 30 min in 0.02 M Na_2CO_3. After washing off the sericin, fibroin was dissolved in 9.5 M LiBr solution and then dialyzed (molecular weight cut-off 3.5 kDa) against 30 mM phosphate buffer pH 7.4 for 6 h at 4 °C. The final concentration of the fibroin solution after dialysis was in the range 0.2–1.5 *w/v*% (depending on the starting fibroin amount), as determined by weighing the remaining solid after drying. The concentration of the obtained SF solution was also determined by UV, using $\varepsilon_{275nm} = 1.064\ cm^{-1}(mg/ml)^{-1}$. For obvious sensitivity reasons all these experiments were performed in D_2O.

4.2. NMR data

NMR experiments were performed at 25° and 12 °C using a 600 MHz Bruker DMX or 500 MHz AvanceII spectrometers equipped with triple resonance TXI probes. Typical ^{1}H 1D NMR spectra were recorded with 64 scans and a spectral width of 7183 Hz. Spectra were referenced to the dioxane signal (3.7 ppm) used as internal standard. Two-dimensional homonuclear TOCSY (mixing 70 ms) and NOESY (mixing 150 ms) experiments were performed at 600 MHz employing standard Bruker library pulse sequences. Matrices of 2048 (t2) by 512 points (t1) were collected. 2D ^{1}H-DOSY experiments were recorded employing the convection-compensated two-dimensional double stimulated echo bipolar pulse (DSTE-BPP) sequence [38]. Matrices of 2048 (t2) by 80 or 128 points (t1) were collected. The z-axis gradient strength was varied linearly from 2 to 98% of its maximum value (53 G/cm). The gradient pulse duration was 2.2 ms, while the time period between the two gradient pulses was set in the range 0.5–1.5 ms to estimate the diffusion time of larger molecules. DOSY experiments optimized for small ligand observation were performed with gradient pulse duration of 2.2 ms and time period between the two gradient pulses set to 45 ms. Water suppression in DOSY experiments was achieved with a standard Bruker library DSTE DOSY sequence with the addition of a sculpting module [39]. DOSY experiments on 0.1 μM SF samples were performed in D_2O. Self-diffusion coefficients were derived by fitting NMR data to Stejskal and Tanner equation [40]. Dioxane (45 μM) was added as internal reference to compare different experiments. This approach also allows minimizing erroneous D estimates deriving from temperature fluctuations and changes in sample viscosity and density. Gradient pulse duration and the time period between the two gradient pulses were set to 2.2 ms and 1 ms, respectively, for the analysis of 1D diffusion measurements at 50% gradient strength for SF samples in the presence of RHD. All spectra were manually phased and baseline corrected using TOPSPIN 4.0.1 (Bruker, Karlsruhe, Germany). Diffusion data were obtained through the Dynamic Centre tool implemented in Topspin 4.0.2 software. Dioxane molecule radius (2.12 Å) was used as standard to obtain estimates of the effective hydrodynamic radius of SF oligomers, assuming a spherical model, using the following equation: $R_h^{SF} = \frac{D_{diox}}{D_{SF}} \times R_h^{diox}$.

4.3. UV absorption measurements

UV absorption spectra were measured using Shimadzu UV-2700 spectrophotometer. The extinction coefficient of silk fibroin in aqueous solution was determined to be $\varepsilon_{275nm} = 1.064\ cm^{-1}(mg/ml)^{-1}$. This value is consistent with previously reported data [41]. Molecular weight of 390 kDa was used to estimate molar concentration of fibroin solution. The concentration of a stock solution of rhodamine 6G was determined using ε (MetOH) = 116,000 $M^{-1}\ cm^{-1}$ [42]. Absorption spectra of RHD in water show maxima around 526.5 nm with a shoulder at 493.0 nm. The increase of RHD concentration results in the formation of aggregates, as deduced from the gradual increase in relative absorptions at 493.0 nm.

4.4. DLS analysis

Dynamic Light Scattering (DLS) measurements were performed at 25 °C using a Zetasizer Nano ZS (Malvern Instruments, Malvern, UK) operating at at λ = 633 nm and equipped with a back scattering detector (173°). Each measurement was the average of 6 or 7 data sets acquired for 10 s.

Conflicts of interest

None.

Transparency document

The http://dx.doi.org/10.1016/j.bbapap.2018.03.009 associated with this article can be found, in online version.

Acknowledgements

Authors acknowledge bilateral project CNR-Azerbaijan National Academy of Sciences (ANAS) 2016-2017 for financial support. HM and LR gratefully acknowledge Fondazione Antonio De Marco (Italy) for financial support.

Author contributions

H.M. and L.R designed and performed the NMR experiments; O.G., A.G., R.A and C·B performed optical measurements; S.Z. performed DLS experiments. H.M., L.R. and O.G. wrote the paper. All authors have given approval to the final version of the manuscript.

Appendix A. Supplementary data

Supplementary data to this article can be found online at https://doi.org/10.1016/j.bbapap.2018.03.009.

References

[1] A. Pistone, A. Sagnella, C. Chieco, G. Bertazza, G. Varchi, F. Formaggio, T. Posati, E. Saracino, M. Caprini, S. Bonetti, S. Toffanin, N. Di Virgilio, M. Muccini, F. Rossi, G. Ruani, R. Zamboni, V. Benfenati, Silk fibroin film from golden-yellow *Bombyx mori* is a biocomposite that contains lutein and promotes axonal growth of primary neurons, Biopolymers 105 (2016) 287–299.
[2] Y. Suzuki, T. Yamazaki, A. Aoki, H. Shindo, T. Asakura, NMR study of the structures of repeated sequences, GAGXGA (X = S, Y, V), in *Bombyx mori* liquid silk, Biomacromolecules 15 (2014) 104–112.
[3] T. Asakura, K. Isobe, A. Aoki, S. Kametani, Conformation of crystalline and non-crystalline domains of [3-C-13]Ala-, [3-C-13]Ser-, and [3-C-13]Tyr-*Bombyx mori* silk fibroin in a hydrated state studied with C-13 DD/MAS NMR, Macromolecules 48 (2015) 8062–8069.
[4] T. Asakura, Y. Sato, A. Aoki, Stretching-induced conformational transition of the crystalline and noncrystalline domains of C-13-labeled *Bombyx mori* silk fibroin monitored by solid state NMR, Macromolecules 48 (2015) 5761–5769.
[5] P. Cebe, B.P. Partlow, D.L. Kaplan, A. Wurm, E. Zhuravlev, C. Schick, Silk I and Silk II studied by fast scanning calorimetry, Acta Biomater. 55 (2017) 323–332.
[6] A. Matsumoto, J. Chen, A.L. Collette, U.J. Kim, G.H. Altman, P. Cebe, D.L. Kaplan, Mechanisms of silk fibroin sol-gel transitions, J. Phys. Chem. B 110 (2006) 21630–21638.
[7] L. Xu, S. Tu, C. Chen, J. Zhao, Y. Zhang, P. Zhou, Effect of EGCG on Fe(III)-induced conformational transition of silk fibroin, a model of protein related to neurodegenerative diseases, Biopolymers 105 (2015) 100–107.
[8] S. Ling, C. Li, J. Adamcik, Z. Shao, X. Chen, R. Mezzenga, Modulating materials by orthogonally oriented beta-strands: composites of amyloid and silk fibroin fibrils, Adv. Mater. 26 (2014) 4569–4574.
[9] J. Greenwald, R. Riek, Biology of amyloid: structure, function, and regulation, Structure 18 (2010) 1244–1260.
[10] L. Jean, A.C. Foley, D.J.T. Vaux, The physiological and pathological implications of the formation of hydrogels, with a specific focus on amyloid polypeptides, Biomol. Ther. 7 (2017).
[11] M. Landreh, J. Johansson, A. Rising, J. Presto, H. Jornvall, Control of amyloid assembly by autoregulation, Biochem. J. 447 (2012) 185–192.
[12] S. Kapoor, S.C. Kundu, Silk protein-based hydrogels: promising advanced materials for biomedical applications, Acta Biomater. 31 (2016) 17–32.
[13] T. Asakura, A. Nishimura, S. Kametani, S. Kawanishi, A. Aoki, F. Suzuki, H. Kaji, A. Naito, Refined crystal structure of *Samia cynthia* ricini silk fibroin revealed by solid-state NMR investigations, Biomacromolecules 18 (2017) 1965–1974.
[14] D.N. Rockwood, R.C. Preda, T. Yucel, X. Wang, M.L. Lovett, D.L. Kaplan, Materials fabrication from *Bombyx mori* silk fibroin, Nat. Protoc. 6 (2011) 1612–1631.
[15] T. Asakura, Y. Watanabe, A. Uchida, H. Minagawa, Nmr of silk fibroin .2. C-13 Nmr-study of the chain dynamics and solution structure of *Bombyx mori* silk fibroin, Macromolecules 17 (1984) 1075–1081.
[16] Z.H. Ayub, M. Arai, K. Hirabayashi, Mechanism of the gelation of fibroin solution, Biosci. Biotechnol. Biochem. 57 (1993) 1910–1912.
[17] U.J. Kim, J. Park, C. Li, H.J. Jin, R. Valluzzi, D.L. Kaplan, Structure and properties of silk hydrogels, Biomacromolecules 5 (2004) 786–792.
[18] T. Asakura, J. Ashida, T. Yamane, T. Kameda, Y. Nakazawa, K. Ohgo, K. Komatsu, A repeated beta-turn structure in poly(Ala-Gly) as a model for silk I of Bombyx mori silk fibroin studied with two-dimensional spin-diffusion NMR under off magic angle spinning and rotational echo double resonance, J. Mol. Biol. 306 (2001) 291–305.
[19] T. Asakura, K. Okushita, M.P. Williamson, Analysis of the structure of *Bombyx mori* silk fibroin by NMR, Macromolecules 48 (2015) 2345–2357.
[20] T. Fujiwara, Y. Kobayashi, Y. Kyogoku, K. Kataoka, Conformational study of ^{13}C-enriched fibroin in the solid state, using the cross polarization nuclear magnetic resonance method, J. Mol. Biol. 187 (1986) 137–140.
[21] K. Numata, D.L. Kaplan, Differences in cytotoxicity of beta-sheet peptides originated from silk and amyloid beta, Macromol. Biosci. 11 (2011) 60–64.
[22] Y. Deng, D. ji, P. Sun, D. Knight, J. Cai, P. Zhou, The role of Mn(II) in silk fibroin based on EPR and NMR spectroscopy, Spectrosc. Lett. 44 (2011) 176–185.
[23] A. Sagnella, C. Chieco, N. Di Virgilio, S. Toffanin, T. Posati, A. Pistone, S. Bonetti, M. Muccini, G. Ruani, V. Benfenati, F. Rossi, R. Zamboni, Bio-doping of regenerated silk fibroin solution and films: a green route for biomanufacturing, RSC Adv. 4 (2014) 33687–33694.
[24] M. Otikovs, G. Chen, K. Nordling, M. Landreh, Q. Meng, H. Jornvall, N. Kronqvist, A. Rising, J. Johansson, K. Jaudzems, Diversified structural basis of a conserved molecular mechanism for pH-dependent dimerization in spider silk N-terminal domains, Chembiochem 16 (2015) 1720–1724.
[25] N. Kronqvist, M. Otikovs, V. Chmyrov, G. Chen, M. Andersson, K. Nordling, M. Landreh, M. Sarr, H. Jornvall, S. Wennmalm, J. Widengren, Q. Meng, A. Rising, D. Otzen, S.D. Knight, K. Jaudzems, J. Johansson, Sequential pH-driven dimerization and stabilization of the N-terminal domain enables rapid spider silk formation, Nat. Commun. 5 (2014) 3254.
[26] R.F. Karlicek, I.J. Lowe, Modified pulsed gradient technique for measuring diffusion in the presence of large background gradients, J. Magn. Reson. 37 (1980) 75–91.
[27] K.F. Morris, C.S. Johnson, Diffusion-ordered 2-dimensional nuclear-magnetic-resonance spectroscopy, J. Am. Chem. Soc. 114 (1992) 3139–3141.
[28] J. Danielsson, J. Jarvet, P. Damberg, A. Graslund, Translational diffusion measured by PFG-NMR on full length and fragments of the Alzheimer a beta(1–40) peptide. Determination of hydrodynamic radii of random coil peptides of varying length, Magn. Reson. Chem. 40 (2002) S89–S97.
[29] S. De, A. Girigoswami, S. Das, Fluorescence probing of albumin-surfactant interaction, J. Colloid Interface Sci. 285 (2005) 562–573.
[30] S. Tomaselli, U. Giovanella, K. Pagano, G. Leone, S. Zanzoni, M. Assfalg, F. Meinardi, H. Molinari, C. Botta, L. Ragona, Encapsulation of a rhodamine dye within a bile acid binding protein: toward water processable functional bio host-guest materials, Biomacromolecules 14 (2013) 3549–3556.
[31] D. Toptygin, B.Z. Packard, L. Brand, Resolution of absorption spectra of rhodamine 6G aggregates in aqueous solution using the law of mass action, Chem. Phys. Lett. 277 (1997) 6.
[32] C.K. Wang, S.E. Northfield, J.E. Swedberg, P.J. Harvey, A.M. Mathiowetz, D.A. Price, S. Liras, D.J. Craik, Translational diffusion of cyclic peptides measured using pulsed-field gradient NMR, J. Phys. Chem. B 118 (2014) 11129–11136.
[33] J.A. Jones, D.K. Wilkins, L.J. Smith, C.M. Dobson, Characterisation of protein unfolding by NMR diffusion measurements, J. Biomol. NMR 10 (1997) 199–203.
[34] D.K. Wilkins, S.B. Grimshaw, V. Receveur, C.M. Dobson, J.A. Jones, L.J. Smith, Hydrodynamic radii of native and denatured proteins measured by pulse field gradient NMR techniques, Biochemistry 38 (1999) 16424–16431.
[35] J. Hrabe, G. Kaur, D.N. Guilfoyle, Principles and limitations of NMR diffusion measurements, J. Med. Phys. 32 (2007) 34–42.
[36] T. Asakura, K. Suita, T. Kameda, S. Afonin, A.S. Ulrich, Structural role of tyrosine in *Bombyx mori* silk fibroin, studied by solid-state NMR and molecular mechanics on a model peptide prepared as silk I and II, Magn. Reson. Chem. 42 (2004) 258–266.
[37] G.D. Mogosanu, A.M. Grumezescu, Natural and synthetic polymers for wounds and burns dressing, Int. J. Pharm. 463 (2014) 127–136.
[38] A. Jerschow, N. Muller, Efficient simulation of coherence transfer pathway selection by phase cycling and pulsed field gradients in NMR, J. Magn. Reson. 134 (1998) 17–29.
[39] A. Jerschow, N. Muller, Suppression of convection artifacts in stimulated-echo diffusion experiments. Double-stimulated-echo experiments, J. Magn. Reson. 125 (1997) 372–375.
[40] E.O. Stejskal, J.E. Tanner, Spin diffusion measurements: spin echoes in the presence of a time-dependent field gradient, J. Chem. Phys. 42 (1965) 5.
[41] M.S. Narasinga Rao, M.W. Pandit, An ultracentrifuge study of silk fibroin, Biochim. Biophys. Acta 94 (1965) 238–247.
[42] R.F. Yunus, Y.-M. Zheng, K.G.N. Nanayakkara, J.P. Chen, Electrochemical removal of rhodamine 6G by using RuO2 coated TiDSA, Ind. Eng. Chem. Res. 48 (2009) 7466–7473.

SUPPORTING INFORMATIONS

Rhodamine binds to silk fibroin and inhibits its self-aggregation

Laura Ragona[a]*, *Oktay Gasymov*[b], *Aytaj J. Guliyeva*[b], *Rasim B. Aslanov*[b], *Serena Zanzoni*[c], *Chiara Botta*[a], *Henriette Molinari*[a]*

[a]Istituto per lo Studio delle Macromolecole (ISMAC), CNR, via Corti 12, 20133 Milano, Italy.

[b]Institute of Biophysics of ANAS, 117 Khalilov, AZ-1141, Baku, Azerbaijan.

[c]Department of Biotechnology, University of Verona, Strada Le Grazie 15, 37134 Verona, Italy.

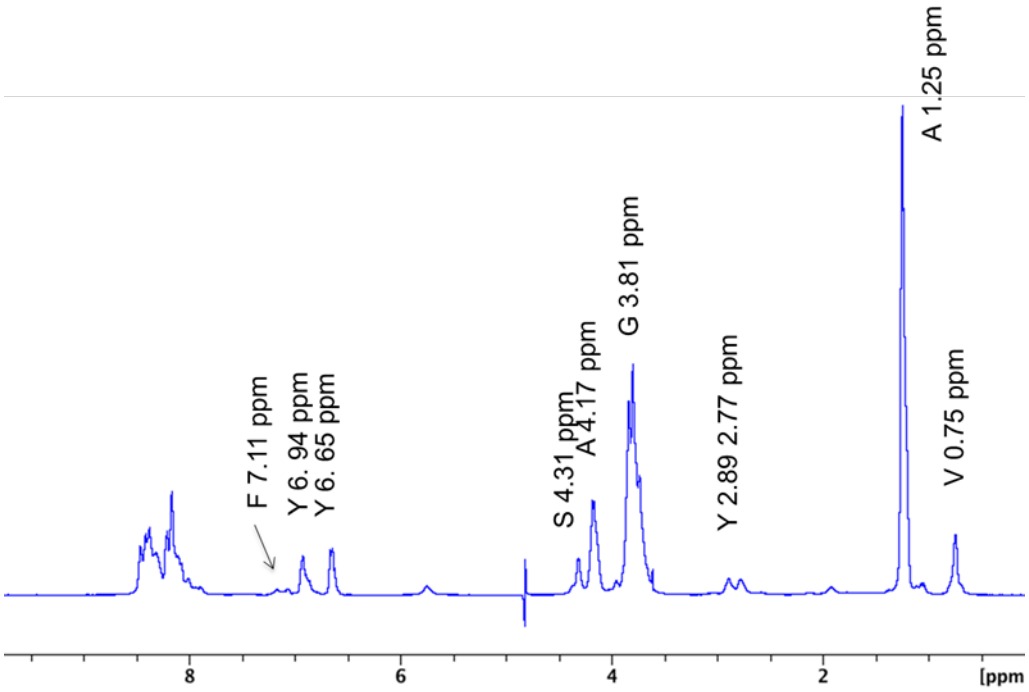

Fig. S1. ^{1}H 1D spectrum of 30μM SF samples at 25°C. Assignments are indicated on the spectrum.

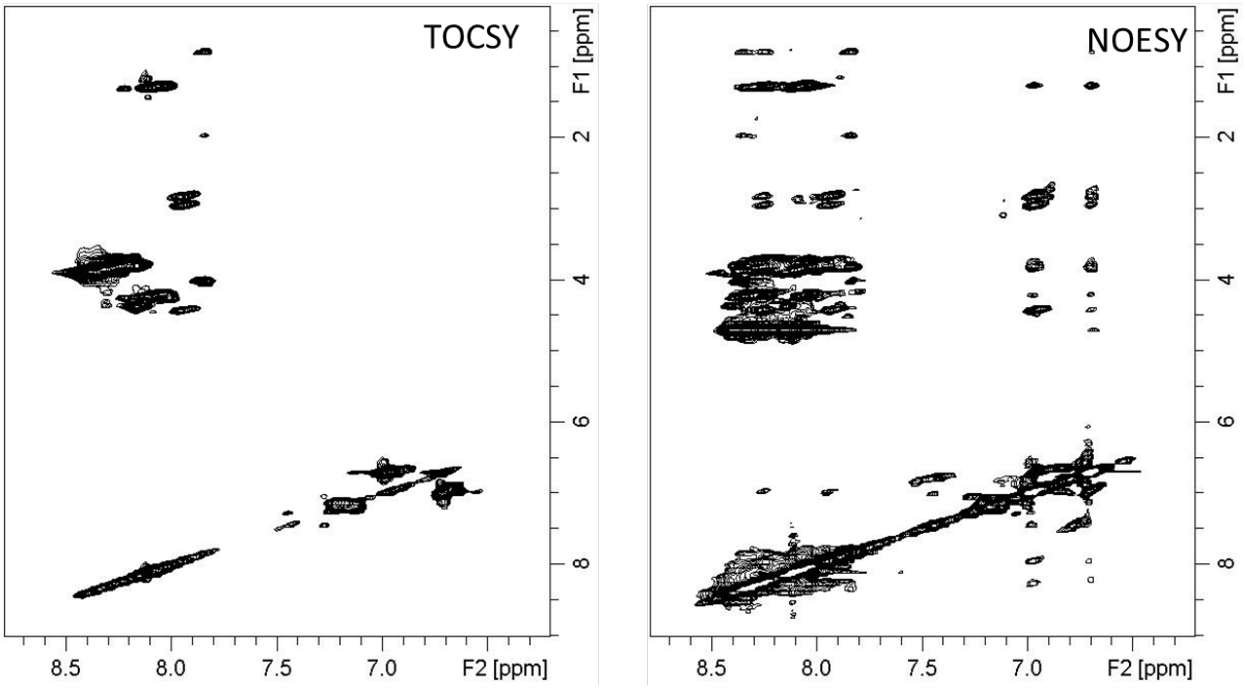

Fig. S2. 2D ^{1}H TOCSY (left panel) and NOESY (right panel) spectra of 30 μM SF samples at 25°C.

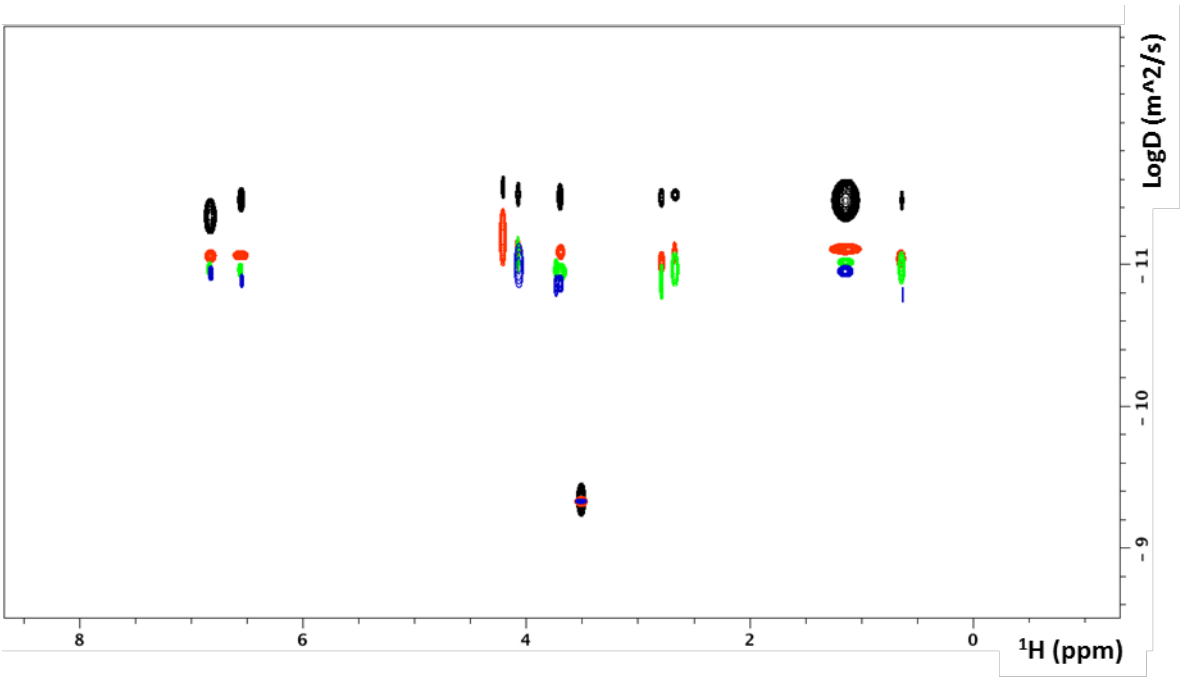

Fig. S3. Superposition of 2D-DOSY spectra of SF samples at 12°C at different concentrations (22 µM black, 11 µM red, 5 µM green, 2.5 µM blue) at pH 6.0. Samples were obtained from dialysis against water.

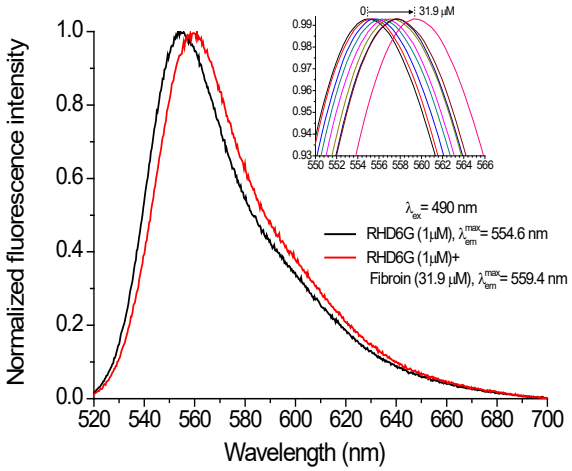

Fig. S4. Fluorescence spectral shift of RHD upon binding to SF. The normalized fluorescence spectra of RHD (1 μM) in 10 mM phosphate buffer pH 7.4 without (black line, fluorescence λ_{max}= 554.6 nm) and with 31.9 μM silk fibroin (red line, fluorescence λ_{max}= 559.4 nm). Inset: gradual fluorescence spectral shift of RHD upon increasing silk fibroin concentration (λ_{ex} = 490 nm). The arrow on the top of the spectra indicates the direction and the range of increase of SF concentration. Graph scale is changed to better visualize the spectral shift. Fluorescence measurements were made on a Tokyo Instruments spectrofluorometer equipped with MS series of monochromator-spectrograph with automatic calibration. Bandwidths for excitation and emission were 2 nm and 4 nm, respectively. Fluorescence spectra were corrected for light scattering from buffer.

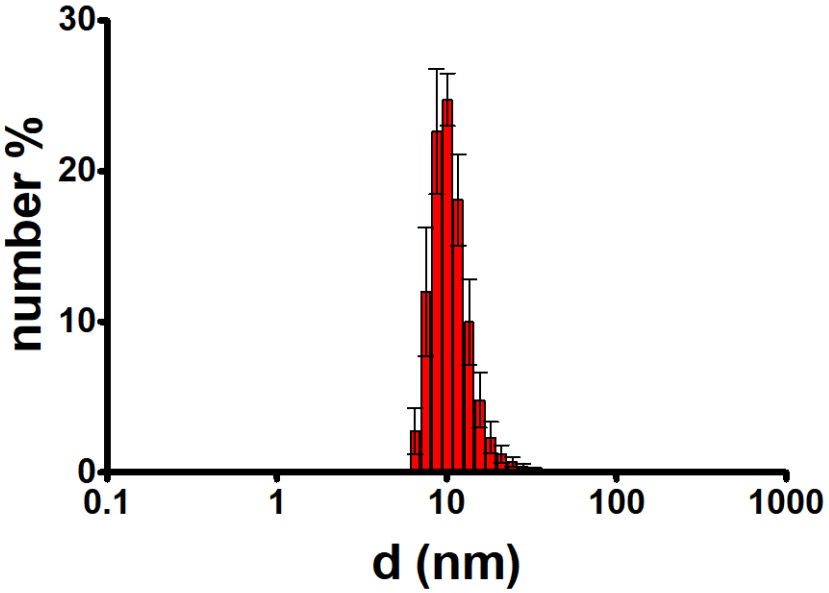

Fig. S5. DLS size distribution of 11 μM SF sample.